JACS
JOURNAL OF THE AMERICAN CHEMICAL SOCIETY
Communication
pubs.acs.org/JACS

Establishing Porosity Gradients within Metal–Organic Frameworks Using Partial Postsynthetic Ligand Exchange

Chong Liu,[†] Chenjie Zeng,[‡] Tian-Yi Luo,[†] Andrea D. Merg,[†] Rongchao Jin,[‡] and Nathaniel L. Rosi*[,†]

[†]Department of Chemistry, University of Pittsburgh, Pittsburgh, Pennsylvania 15260, United States
[‡]Department of Chemistry, Carnegie Mellon University, Pittsburgh, Pennsylvania 15213, United States

Supporting Information

ABSTRACT: Crystalline 3-D materials bearing interlinked domains of differential porosity and functionality offer the potential for organizing and shuttling molecular and nanoscale matter to specific locations within 3-D space. Here, we present methods for creating prototype MOF materials that have such structural features. Specifically, the process of pore expansion via ligand exchange was studied for an isoreticular series of mesoporous MOFs based on **bMOF-100**. It was found that pore expansion occurs incrementally in small steps and that it proceeds gradually in an "outside→in" fashion within individual crystals. The ligand exchange reaction can be terminated prior to complete crystal conversion to yield intermediate product MOFs, denoted **bMOF-100/102** and **bMOF-102/106**, which bear descending porosity gradients from the crystal periphery to the crystal core. As a proof of concept, size-sensitive incorporation of a gold–thiolate nanocluster, $Au_{133}(SR)_{52}$, selectively in the **bMOF-102/106** crystal periphery region was accomplished via cation exchange. These new methods open up the possibility of controlling molecular organization and transport within porous MOF materials.

Constructing MOFs with organized domains or strata of differential porosity is a significant challenge.[1] Controlled installation of pores of different dimensions[2] may ultimately allow for controllable flow of analytes from domain to domain within a MOF crystal. Further, it may enable selective placement of molecules within the crystal based on geometrical parameters such as kinetic diameter. Numerous methods have been reported for introducing structural and functional heterogeneity into otherwise homogeneous MOF crystals.[3] However, challenges remain in predicting and identifying the patterns of achievable structural and functional heterogeneity.[4] Established methods usually lack spatial and compositional control over the heterogeneous components in MOFs, with the exception of crystal overgrowth methods which have been thoroughly studied.[1,3i−l] Core–shell MOFs and other layered MOFs have been prepared, wherein the layers are typically crystallographically compatible.[1a−c,3i−l]

Here, we report the rational control of pore size expansion within the mesoporous **bMOF-100** series MOF crystals via ligand exchange. We determine that pore expansion occurs regionally and directionally in an "outside→in" fashion. Finally, we use this phenomenon to create MOF crystals with identifiable domains of differential porosity and directional pore size gradients.

We previously demonstrated that stepwise ligand exchange could be used to increase incrementally the pore size of mesoporous **bMOF-100** crystals by replacing the original ligands with longer ligands.[5] This study was the first example of using ligand exchange to increase MOF pore dimensions. The observed pore expansion phenomenon was fundamentally interesting because **bMOF-100** is a cubic crystal; therefore, ligand exchange and pore expansion must occur in three dimensions.[6] We note that other ligand exchange based pore expansion studies have since been reported for pillared MOFs, wherein the MOF is expanded in only a single dimension.[7] Given the unique aspects of the **bMOF-100** system, we endeavored to explore the ligand exchange based pore expansion process in greater detail in order to push the dimension limits of pore expansion and gain an understanding of the process.

The following sequential pore expansion process has been realized: **bMOF-100** → **bMOF-102** → **bMOF-106** → **bMOF-107** (Figure 1A and S8). **bMOF-106** and **bMOF-107** represent new additions to this isoreticular series. In this series, **bMOF-100** ($Zn_8(ad)_4(BPDC)_6O_2$·4cation, ad = adeninate, BPDC = biphenyl-4,4′-dicarboxylate, cation = dimethylammonium) crystals were converted to **bMOF-102** crystals via exchanging BPDC with azobenzene-4,4′-dicarboxylate (ABDC); the as-produced **bMOF-102** crystals were converted to **bMOF-106** crystals through exchange of ABDC with 2′-nitro-1,1′:4′,1″-terphenyl-4,4″-dicarboxylate (NO_2-TPDC); and finally the as-produced **bMOF-106** crystals were converted to **bMOF-107** through exchange of NO_2-TPDC with 4-(3′-nitro-4′-(4″-carboxylphenylethynyl)phenyl)benzoate (NO_2-eTPDC) (see Supporting Information for details). Unit cell parameters for the product crystalline materials were collected (Supporting Information Section 4.6) and model structures were constructed using these data (Figures S14–S16). Complete structural conversion via ligand exchange was confirmed by comparing the experimental powder X-ray diffraction (PXRD) patterns of the product materials to simulated PXRD patterns generated from the model structures (Figures 1B and S9). The composition of the product materials, after copious washing to remove unreacted and exchanged ligands, was determined via analysis of proton nuclear magnetic resonance (^{1}H NMR) spectra of dissolved samples (Figure 1C). In each case, ligand

Received: July 21, 2016
Published: September 3, 2016

DOI: 10.1021/jacs.6b07445
J. Am. Chem. Soc. 2016, 138, 12045−12048

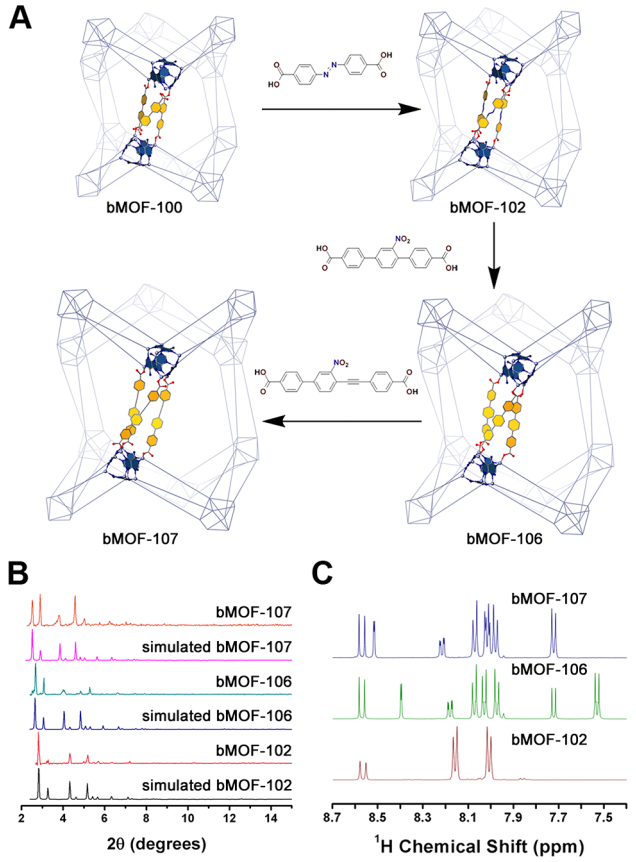

Figure 1. (A) Schematic representation of sequential pore expansion from **bMOF-100** to **bMOF-102** to **bMOF-106** to **bMOF-107** via ligand exchange. (B) PXRD comparing MOFs made from ligand exchange with simulated patterns from model structures. (C) ^{1}H NMR spectra revealing the ligand composition of MOFs prepared via ligand exchange.

exchange is virtually complete (>97% exchange). The mechanism of exchange (e.g., associative/dissociative) is yet to be determined, but it is known that the coordination capabilities of incoming ligands have a direct impact on the rate and extent of ligand exchange.[7,8] We note that the structural conversion from **bMOF-102** to **bMOF-106** is similar to the previously reported expansion from **bMOF-102** to **bMOF-103**;[5] however, conversion from **102** to **106** is significantly faster and more complete than the conversion from **102** to **103**. The only difference between the two reactions is the functional group on the terphenyldicarboxylic acid: an electron donating amino group for **103** and an electron withdrawing nitro group for **106**. This difference highlights the importance of ligand acidity (i.e., concentration of coordination sites) for ligand exchange in this system, where more acidic ligands accelerate the process. We therefore surmise that the reaction is kinetically controlled. For crystals with the same average size, close monitoring of the reaction with ^{1}H NMR revealed that ligand replacement proceeded gradually, as detected by the gradually increasing presence of the longer linker in the product material (Figure S5).

All attempts to convert directly **bMOF-100** to **106** or **102** to **107** failed (Figure S10, see Supporting Information Section 4.5 for details). In these cases, the framework remained unexpanded and did not contain the longer ligands, as evidenced by PXRD (Figure S11) and ^{1}H NMR (Figure S12), respectively. Therefore, it is concluded that, for this system, MOF pore expansion via ligand exchange is only successful if the ligand length is incrementally increased (<∼0.3 nm length change). We can deduce from these results that structure conversion occurs through ligand exchange in the solid-state material rather than through a dissolution/recrystallization process, because the latter process would presumably accommodate any ligand length provided that the linker could form an isoreticular MOF. The pores in this series are sufficiently large (>2 nm in diameter) and continuous, so we do not expect ligand diffusion to be an issue; indeed, we have shown previously that very large molecules (larger than the ligands used in this study) can diffuse readily throughout the 3-D pore space of **bMOF-100**.[4d,9] We can also infer that the 3-D structure of these MOFs are somewhat flexible and can tolerate strain associated with gradual replacement of shorter ligands with longer ligands.

Having demonstrated that incremental stepwise pore expansion is feasible for the **bMOF-100** series, we next proceeded to determine whether the ligand exchange process occurs homogeneously throughout the crystal (i.e., simultaneously in all regions of the crystal) or heterogeneously (i.e., gradually from domain to domain). Large **bMOF-100** crystals were synthesized under modulated solvothermal conditions (Supporting Information Section 3) and the ligand exchange reaction to produce **bMOF-102** was allowed to proceed for 10 min before it was terminated (Figure 2A). The composition and structure of the product crystals were analyzed. Based on ^{1}H NMR analysis, 38.7% of the BPDC ligands were exchanged with ABDC (Figure S5). A large crystal was carefully fractured. It is clear from optical microscopy images (Figure 2C) that the crystal periphery bears the orange color characteristic of the ABDC ligand and the crystal core remains colorless. Microspectrophotometric measurements were conducted for different regions of a sliced intermediate **bMOF-100/102** crystal (Figure S13), starting at the core and moving to the periphery. The absorbance spectra indicate that the crystal, from the core to the periphery, gradually exhibits more **bMOF-102** character. Inspired by X-ray diffraction studies that monitor MOF transformations,[10] unit cell data were collected for the orange periphery fraction and the colorless core (Figure 2B). These data suggest that the ligands are distributed in a gradient fashion from ABDC to BPDC from the periphery to the core, respectively; that is, the periphery contains more **bMOF-102** character (larger unit cell) and the core contains more **bMOF-100** character (smaller unit cell). Similar experiments were performed for the **bMOF-102/106** system and the data also suggest that ligand exchange begins at the periphery and proceeds toward the core (Figure 2D–F). From these results, we conclude that pore expansion via ligand exchange proceeds in an "outside→in" fashion. The interesting implication of this finding is that we can use this process to produce MOF crystals with pore gradients that have larger pores in their periphery and smaller pores in their core.

Crystals exhibiting domains with different pore dimensions present the opportunity of organizing nanoscale species in a hierarchical fashion based on size. It is anticipated that in MOF crystals with a 3-D pore gradient, guest species of precise size should only penetrate to a certain depth, resulting in a heterogeneous distribution. Gold–thiolate nanoclusters were chosen as guest species because of their precise dimensions and interesting physical properties.[11] Further, their UV–Vis spectra are discernible from those of the MOF, which should enable

DOI: 10.1021/jacs.6b07445
J. Am. Chem. Soc. 2016, 138, 12045–12048

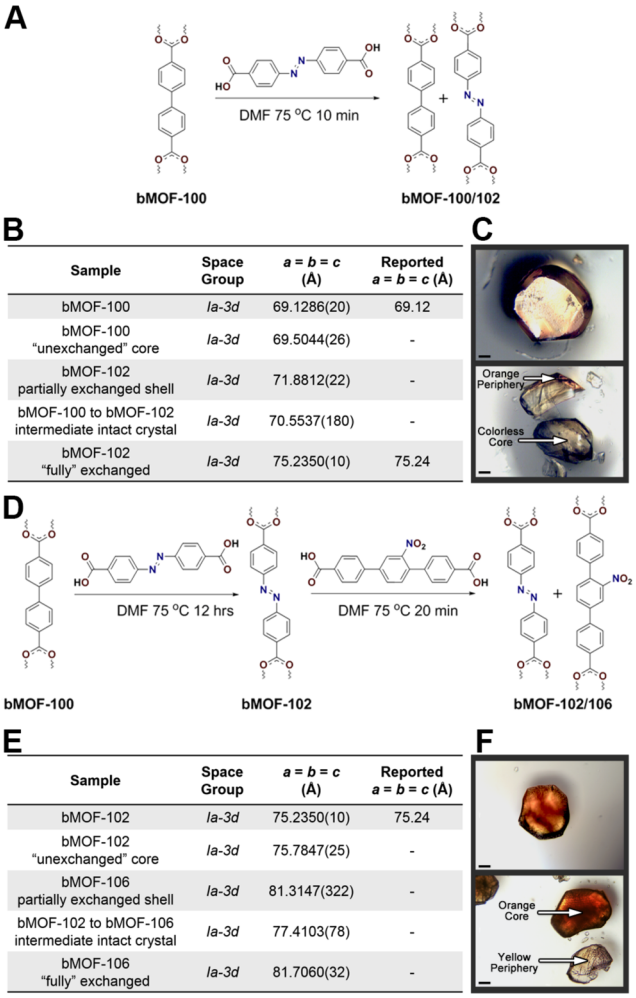

Sample	Space Group	$a = b = c$ (Å)	Reported $a = b = c$ (Å)
bMOF-100	*Ia-3d*	69.1286(20)	69.12
bMOF-100 "unexchanged" core	*Ia-3d*	69.5044(26)	-
bMOF-102 partially exchanged shell	*Ia-3d*	71.8812(22)	-
bMOF-100 to bMOF-102 intermediate intact crystal	*Ia-3d*	70.5537(180)	-
bMOF-102 "fully" exchanged	*Ia-3d*	75.2350(10)	75.24

Sample	Space Group	$a = b = c$ (Å)	Reported $a = b = c$ (Å)
bMOF-102	*Ia-3d*	75.2350(10)	75.24
bMOF-102 "unexchanged" core	*Ia-3d*	75.7847(25)	-
bMOF-106 partially exchanged shell	*Ia-3d*	81.3147(322)	-
bMOF-102 to bMOF-106 intermediate intact crystal	*Ia-3d*	77.4103(78)	-
bMOF-106 "fully" exchanged	*Ia-3d*	81.7060(32)	-

Figure 2. (A) Ligand exchange reaction to yield gradient **bMOF-100/102**. (B) Table comparing unit cell parameters for **bMOF-100/102** system. (C) Optical image showing an intact crystal (top) and manually separated "core" and "shell" (bottom), scale bar 50 μm. (D) Ligand exchange reaction to yield gradient **bMOF-102/106**. (E) Table comparing unit cell parameters for **bMOF-102/106** system. (F) Optical image showing an intact crystal (top) and manually separated "core" and "shell" (bottom), scale bar 100 μm.

determination of their relative positions within the 3-D crystal via spectral microscopy.

The **bMOF-102/106** gradient MOF and $Au_{133}(SR)_{52}$, icosahedral nanocluster with an overall diameter of 3 nm (gold core plus ligand shell)[12] were used as host and guest respectively for proof of principle studies. On the basis of its diameter, we predicted that $Au_{133}(SR)_{52}$ should locate exclusively in the periphery of the **bMOF-102/106** gradient MOF that has **106** pore character (Figure 3A). We note that the **bMOF-100** series of MOFs is anionic, and dimethylammonium cations reside in the pores. Thus, cation exchange can be an effective means of introducing new guest species to the pore space. To enable cation exchange-driven diffusion, the Au nanoclusters were oxidized with H_2O_2 (Supporting Information Section 5.1).[13] Control experiments were performed using **bMOF-102** and **bMOF-106** single crystals, respectively. MOF samples were treated with identical dichloromethane solutions of $Au_{133}(SR)_{52}^+$ for the same period of time. The absorbance spectra of the supernatants were monitored (Figures S18 and S19) to determine the extent of cluster uptake into the MOF

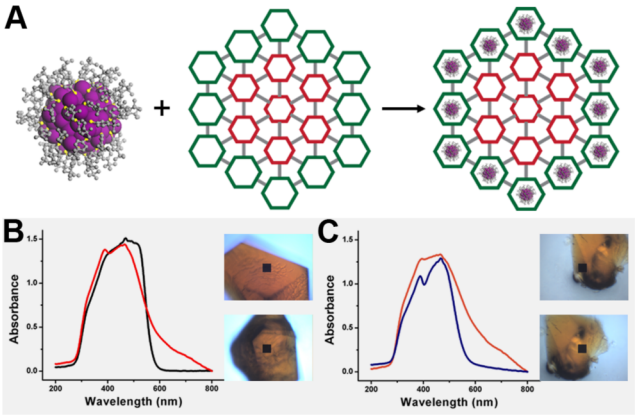

Figure 3. (A) Schematic representation of "ideal" $Au_{133}(SR)_{52}$ organization in the periphery of gradient **bMOF-102/106**. (B) Absorbance spectra of **bMOF-102/106** before (black) and after (red) encapsulation of $Au_{133}(SR)_{52}$ and corresponding optical images (before, top; after, bottom). (C) Absorbance spectra of different regions of a **bMOF-102/106** crystal showing the presence of $Au_{133}(SR)_{52}$ in the periphery (orange) but not the core (blue) and corresponding optical images (periphery, top; core, bottom). For all optical images, black squares (37 × 37 μm^2) indicate sampling area for absorbance spectroscopy.

samples. It is clear from these data that $Au_{133}(SR)_{52}^+$ diffused more readily into **bMOF-106** than into **bMOF-102**, which has a pore diameter (~2.9 nm) slightly less than the cluster diameter. Microspectrophotometric results (Figure S20) show that $Au_{133}(SR)_{52}^+$ penetrates to all regions of the **bMOF-106** crystals, indicating that the crystals are sufficiently porous to allow for diffusion throughout the material and, importantly, revealing that the nanoclusters do not clog the pores and prevent further diffusion. $Au_{133}(SR)_{52}^+$-charged **bMOF-106** was then dissolved to extract the $Au_{133}(SR)_{52}^+$. UV–vis spectroscopy and matrix assisted laser desorption ionization time-of-flight (MALDI-TOF) mass spectrometry confirmed that $Au_{133}(SR)_{52}^+$ remains unchanged throughout the uptake/release process (Figures S21 and S22). Having determined that $Au_{133}(SR)_{52}^+$ can enter **bMOF-106** but not **bMOF-102** and that it remains intact throughout the course of the uptake experiments, we next treated the **bMOF-102/106** with $Au_{133}(SR)_{52}^+$ in the same fashion as described above. The absorbance spectrum recorded for the gradient crystals after treatment with $Au_{133}(SR)_{52}^+$ show new features characteristic of $Au_{133}(SR)_{52}^+$ (Figure 3B). Spectra of fractured gradient crystals loaded with $Au_{133}(SR)_{52}^+$ reveals that the clusters reside exclusively in the periphery (Figure 3C).

In summary, we determined that ligand exchange-facilitated pore expansion of 3-D **bMOF-100** and its analogues is a gradual process that proceeds via ligand replacement from the crystal periphery to the crystal core. Upon halting the ligand exchange reaction, we successfully prepared new heterogeneously porous MOFs with internal pore gradients. The hierarchical distribution of porosity was used for heterogeneous placement of Au nanoclusters. We demonstrated for the first time that postsynthetic ligand exchange can be used to create structurally heterogeneous MOF crystals with internal directional porosity gradients. The realization of porosity gradients now permits size-selective spatial organization of molecular and nanoscale entities within MOF scaffolds and presents new opportunities for creating functional gradients in MOFs that

DOI: 10.1021/jacs.6b07445
J. Am. Chem. Soc. 2016, 138, 12045–12048

can potentially be used for controlling the distribution and flow of matter throughout 3-D ordered molecular space.

■ ASSOCIATED CONTENT

Supporting Information

The Supporting Information is available free of charge on the ACS Publications website at DOI: 10.1021/jacs.6b07445.

Experimental details and additional data (PDF)
Data for $C_{16}H_{10}BrNO_4$ (CIF)
Data for $C_{24}H_{17}NO_6$ (CIF)

■ AUTHOR INFORMATION

Corresponding Author

*nrosi@pitt.edu

Notes

The authors declare no competing financial interest.

■ ACKNOWLEDGMENTS

This project received support from the Defense Threat Reduction Agency-Joint Science and Technology Office for Chemical and Biological Defense Basic Research (Grant no. HDTRA1-16-1-0044, N.L.R.). The authors thank the Petersen Nano Fabrication and Characterization Facility for access to PXRD and microspectrophotometry instrumentation, Dr. Steven J. Geib and Dr. Chen Zhang for helpful discussion, and Ms. Disi Wang for help with figure preparation.

■ REFERENCES

(1) (a) Hirai, K.; Furukawa, S.; Kondo, M.; Uehara, H.; Sakata, O.; Kitagawa, S. *Angew. Chem., Int. Ed.* **2011**, *50*, 8057. (b) Li, T.; Sullivan, J. E.; Rosi, N. L. *J. Am. Chem. Soc.* **2013**, *135*, 9984. (c) Wang, Z.; Liu, J.; Lukose, B.; Gu, Z.; Weidler, P. G.; Gliemann, H.; Heine, T.; Wöll, C. *Nano Lett.* **2014**, *14*, 1526. (d) Choi, K. M.; Park, J. H.; Kang, J. K. *Chem. Mater.* **2015**, *27*, 5088.

(2) (a) Cohen, S. M. *Chem. Rev.* **2012**, *112*, 970. (b) Li, B.; Chrzanowski, M.; Zhang, Y.; Ma, S. *Coord. Chem. Rev.* **2016**, *307*, 106.

(3) (a) Furukawa, H.; Muller, U.; Yaghi, O. M. *Angew. Chem., Int. Ed.* **2015**, *54*, 3417. (b) Deng, H.; Doonan, C. J.; Furukawa, H.; Ferreira, R. B.; Towne, J.; Knobler, C. B.; Wang, B.; Yaghi, O. M. *Science* **2010**, *327*, 846. (c) Fracaroli, A. M.; Siman, P.; Nagib, D. A.; Suzuki, M.; Furukawa, H.; Toste, F. D.; Yaghi, O. M. *J. Am. Chem. Soc.* **2016**, *138*, 8352. (d) Karagiaridi, O.; Bury, W.; Mondloch, J. E.; Hupp, J. T.; Farha, O. K. *Angew. Chem., Int. Ed.* **2014**, *53*, 4530. (e) Deria, P.; Mondloch, J. E.; Karagiaridi, O.; Bury, W.; Hupp, J. T.; Farha, O. K. *Chem. Soc. Rev.* **2014**, *43*, 5896. (f) Hong, D. H.; Suh, M. P. *Chem. - Eur. J.* **2014**, *20*, 426. (g) DeCoste, J. B.; Rossin, J. A.; Peterson, G. W. *Chem. - Eur. J.* **2015**, *21*, 18029. (h) He, Y.; Shang, J.; Gu, Q.; Li, G.; Li, J.; Singh, R.; Xiao, P.; Webley, P. A. *Chem. Commun.* **2015**, *51*, 14716. (i) Furukawa, S.; Hirai, K.; Nakagawa, K.; Takashima, Y.; Matsuda, R.; Tsuruoka, T.; Kondo, M.; Haruki, R.; Tanaka, D.; Sakamoto, H.; Shimomura, S.; Sakata, O.; Kitagawa, S. *Angew. Chem., Int. Ed.* **2009**, *48*, 1766. (j) Koh, K.; Wong-Foy, A. G.; Matzger, A. J. *Chem. Commun.* **2009**, 6162. (k) Tang, J.; Salunkhe, R. R.; Liu, J.; Torad, N. L.; Imura, M.; Furukawa, S.; Yamauchi, Y. *J. Am. Chem. Soc.* **2015**, *137*, 1572. (l) Zhuang, J.; Chou, L. Y.; Sneed, B. T.; Cao, Y.; Hu, P.; Feng, L.; Tsung, C. K. *Small* **2015**, *11*, 5551. (m) McGuire, C. V.; Forgan, R. S. *Chem. Commun.* **2015**, *51*, 5199.

(4) (a) Furukawa, S.; Hirai, K.; Takashima, Y.; Nakagawa, K.; Kondo, M.; Tsuruoka, T.; Sakata, O.; Kitagawa, S. *Chem. Commun.* **2009**, 5097. (b) Kong, X.; Deng, H.; Yan, F.; Kim, J.; Swisher, J. A.; Smit, B.; Yaghi, O. M.; Reimer, J. A. *Science* **2013**, *341*, 882. (c) Katzenmeyer, A. M.; Canivet, J.; Holland, G.; Farrusseng, D.; Centrone, A. *Angew. Chem., Int. Ed.* **2014**, *53*, 2852. (d) Liu, C.; Luo, T. Y.; Feura, E. S.; Zhang, C.; Rosi, N. L. *J. Am. Chem. Soc.* **2015**, *137*, 10508.

(5) Li, T.; Kozlowski, M. T.; Doud, E. A.; Blakely, M. N.; Rosi, N. L. *J. Am. Chem. Soc.* **2013**, *135*, 11688.

(6) An, J.; Farha, O. K.; Hupp, J. T.; Pohl, E.; Yeh, J. I.; Rosi, N. L. *Nat. Commun.* **2012**, *3*, 604.

(7) Karagiaridi, O.; Bury, W.; Tylianakis, E.; Sarjeant, A. A.; Hupp, J. T.; Farha, O. K. *Chem. Mater.* **2013**, *25*, 3499.

(8) Karagiaridi, O.; Bury, W.; Sarjeant, A. A.; Stern, C. L.; Farha, O. K.; Hupp, J. T. *Chem. Sci.* **2012**, *3*, 3256.

(9) Liu, C.; Li, T.; Rosi, N. L. *J. Am. Chem. Soc.* **2012**, *134*, 18886.

(10) Zhang, J.-P.; Liao, P.-Q.; Zhou, H.-L.; Lin, R.-B.; Chen, X.-M. *Chem. Soc. Rev.* **2014**, *43*, 5789.

(11) Qian, H.; Zhu, M.; Wu, Z.; Jin, R. *Acc. Chem. Res.* **2012**, *45*, 1470.

(12) Zeng, C.; Chen, Y.; Kirschbaum, K.; Appavoo, K.; Sfeir, M. Y.; Jin, R. *Sci. Adv.* **2015**, *1*, e1500045.

(13) Zhu, M.; Aikens, C. M.; Hendrich, M. P.; Gupta, R.; Qian, H.; Schatz, G. C.; Jin, R. *J. Am. Chem. Soc.* **2009**, *131*, 2490.

DOI: 10.1021/jacs.6b07445
J. Am. Chem. Soc. 2016, 138, 12045−12048